ELSEVIER

Physica C 317–318 (1999) 396–402

PHYSICA C

Observation of paramagnetic Meissner currents—evidence for Andreev bound surface states

W. Prusseit [a,*], H. Walter [b], R. Semerad [b], H. Kinder [b], W. Assmann [c], H. Huber [c], B. Kabius [d], H. Burkhardt [e], D. Rainer [e], J.A. Sauls [f]

[a] *THEVA Dünnschichttechnik, Hauptstrasse 1b, D-85386 Eching-Dietersheim, Germany*
[b] *Physik Department E10, TU München, D-85747 Garching, Germany*
[c] *Sektion Physik, LMU München, D-85748 Garching, Germany*
[d] *IFF, FZ Jülich, 52425 Jülich, Germany*
[e] *Physikalisches Institut, Universität Bayreuth, D-95440 Bayreuth, Germany*
[f] *Department of Physics and Astronomy, Northwestern University, Evanston, IL 60208, USA*

Abstract

We report the observation of anomalous Meissner currents (AMCs) in thin films of superconducting YBCO with oriented internal surfaces introduced by heavy-ion bombardment. High-precision measurements of the penetration depth $\lambda(T)$ reveal an upturn in the temperature dependence of $\lambda(T)$ below $T \approx 15$ K, which is strongly dependent on the orientation and density of the surfaces. The magnitude of the observed effect, its onset temperature and its dependence on the orientation of the surfaces are in quantitative agreement with the theory of surface effects in d-wave superconductors. The anomaly is interpreted as a consequence of surface-induced Andreev bound states (ABSs) carrying paramagnetic currents.

PACS: 74.25.Nf; 74.50.+r; 74.72.Bk

Keywords: Penetration depth; d-Wave superconductors; Andreev scattering

The traditional theory of superconductivity in Fermi liquids predicts that superconductors with anisotropic pairing should react sensitively to surface scattering. As a result, surfaces are expected to be covered by a layer of thickness of a few coherence lengths of strongly distorted superconductivity with properties different from those of the bulk. These anomalous surface phenomena were first discussed in the context of p-wave pairing in ^{3}He [1], later extended to anisotropic pairing in heavy-fermion superconductors [2], and recently, to d-wave pairing in cuprate high-T_c superconductors [3–9]. Typical anomalies are suppression of the order parameter ('surface pair-breaking'), zero-bias peaks in the tunneling conductance, anomalous currents flowing in the 'wrong' direction relative to the diamagnetic Meissner current (DMC), and spontaneous breaking of time reversal symmetry by the surface order parameter [5–7,10,11]. Recent tunneling experiments

* Corresponding author. Tel.: +49-89-32929-176; Fax: +49-32929-177; E-mail: prusseit@theva.com

0921-4534/99/$ - see front matter
PII: S0921-4534(99)00086-6

[12] report the observation of the zero-bias peak for tunneling into the a–b plane, its evolution in a magnetic field, and evidence for a phase transition to a surface state with spontaneously broken time-reversal symmetry. The origin of the surface anomalies is a subtle trapping mechanism of quasiparticles. Quasiparticles which bounce off a surface can be 'retro-reflected' back by Andreev scattering, and repeated reflections lead to Andreev bound states (ABSs). Andreev scattering is sensitive to the anisotropy, phase, and amplitude of the order parameter. Hence, measurements which probe the ABSs may be used to identify the type of superconducting order parameter, both in the bulk and near surfaces.

This paper presents a systematic experimental study of the 'anomalous Meissner current' (AMC), together with a theoretical interpretation of the data. The AMC is carried by ABSs, and has, in addition to its reversed flow direction, the following signatures. It is confined to a distance of a few coherence lengths ($\xi_0 \approx 15$ Å in YBCO) from the surface, and is therefore a small correction to the total screening current, which is in usual experiments dominated by the regular DMC flowing within a penetration depth ($\lambda \approx 1500$ Å in YBCO). The scale for the temperature dependence of the AMC is set by the splitting or width, δ, of the ABSs, and not by the average gap, Δ, which sets the temperature scale for the DMC. One expects $\delta \ll \Delta$, and therefore, a characteristically different temperature dependence of the anomalous and regular Meissner currents. In addition, the magnitude of the AMC depends in a characteristic way on the orientation of the surface with respect to the order parameter. All of these signatures were observed in the experiments described below. We interpret these results as evidence for an AMC caused by ABSs. Since Andreev scattering and ABSs are unique features of the Fermi liquid theory of superconductivity, we also consider these observations to be strong evidence in support of the Fermi-liquid theory for superconductivity with a $d_{x^2-y^2}$ order parameter in cuprate high-T_c superconductors.

The purpose of our experiments was to study the thin layer of strongly distorted superconductivity which is predicted to cover surfaces of $d_{x^2-y^2}$ superconductor, and to measure the sensitivity of these effects to the orientation of the surface. A direct way to detect the surface anomalies associated with ABSs is to measure the low temperature penetration depth of a sample containing a high density of oriented boundaries. The small size of the surface layers, of order ξ_0, requires the preparation of sharp surfaces on the scale of the coherence length, which poses major experimental difficulties. Photolithographic or related patterning techniques are ruled out since degradation at the edges limits the resolution to, at best, 10 nm. Alternatives, based on artificial grain boundaries such as step edge or bicrystal junctions, have orientation problems. Strong faceting on a nanometer scale leads to averaging over many directions and renders the orientation-dependent signatures unobservable [13]. For these reasons, we pursued an unconventional approach, and used ion tracks generated by high-energy heavy-ion bombardment to introduce artificial interfaces [14]. We used epitaxial YBCO films with the c-axis direction perpendicular to the substrate surface. YBCO films were simultaneously grown on batches of eight $20 \times 20 \times 0.5$ mm^3 YSZ (100) substrates by thermal co-evaporation [15]. The films were covered by 10 nm thick Y_2O_3 layers in situ to prevent contact with ambient moisture and long-term degradation. As grown films with a thickness of 80 nm exhibited sharp inductive transitions at 87 K. Prior to ion irradiation, a 300 nm thick AuO_x-mask was deposited by sputtering onto the films to provide a rectangular 5×7 mm^2 wide irradiation window. Insulating AuO_x was chosen because it is most effective in stopping the ion beam within the mask thickness without affecting the inductive measurements below the mask. Ion tracks were generated using 270 MeV Au^{18+} ions from a Tandem accelerator with a beam diameter of 10 mm. A cross-sectional and plan view of the irradiation geometry is depicted in Fig. 1. The beam was directed towards the film surface under a grazing incidence angle of 1.5° (cf. Fig. 1a). The samples were irradiated with fluencies between 1 and 4.5×10^{11} ions/cm^2 along specific directions in the a–b plane of YBCO, i.e., specific orientations with respect to the d-wave order parameter as shown in Fig. 1b. The range of the Au-ions is about 10 μm and is sufficient to penetrate the entire thickness of the YBCO film, leading to 1.5–3 μm straight tracks. The transmission electron microscopy (TEM) cross-section (Fig. 2) of an irradiated 40-nm thick YBCO film reveals that the tracks consist of a slightly

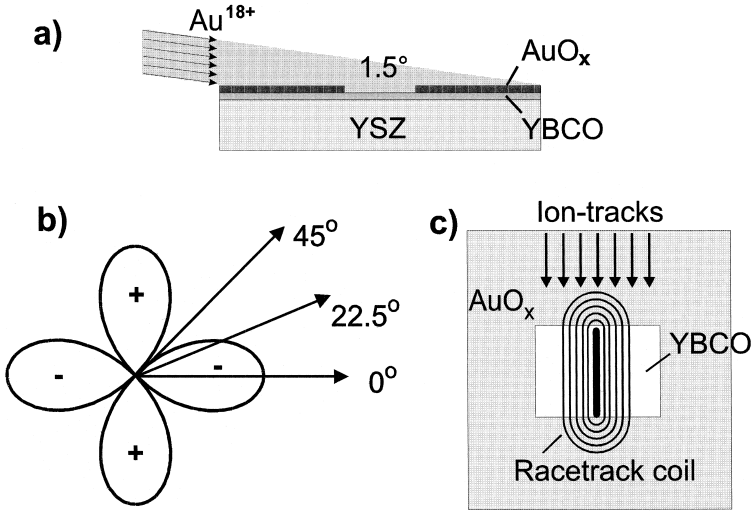

Fig. 1. Irradiation and measurement geometry. (a) Au^{18+} ions impact under grazing incidence onto the YBCO film. The AuO_x layer defines a 5×7 mm^2 wide irradiation window in which the underlying YBCO film is threaded by irradiation tracks; (b) the arrows show the orientation of the three irradiation track directions with respect to the d-wave order parameter; (c) position of the racetrack coils with respect to the irradiated window and the ion beam direction.

elliptical amorphized core region of 12–20 nm diameter. The transition to the surrounding single crystalline material is abrupt within 1–2 nm. A 3–4 nm thick oxygen-deficient layer cannot be ruled out from the TEM survey. Actually, θ–2θ X-ray scans prior and after irradiation revealed that the $(00n)$ peaks developed a small shoulder towards longer *c*-axis lattice parameter upon irradiation, implying some oxygen loss within the affected volume. In the case shown, the average spacing of 30 nm between the tracks is consistent with the applied dose of 10^{11} ions/cm^2. Although a large volume fraction of the YBCO film is radiation damaged, the inductively measured transition temperatures drop by only 2–3 K, suggesting that the residual crystalline material visible in the TEM micrograph has obviously maintained its original properties. The magnetic penetration depth, or more generally, the magnetic field response, is determined by a mutual inductance technique described in detail in Ref. [16]. The YBCO film sample is placed between flat pickup and excitation coils operated at 30 kHz. The excitation field, $B \approx 20$–40 μT, is much smaller than B_{c1} so that the film remains in the Meissner state throughout the measurement. The ratio of the induced voltages in the pickup coil below and above the superconducting transition gives the inverse screening factor $S^{-1}(\lambda)$ which is a monotonic function of the London penetration depth $\lambda(T)$. For simple coil geometries (e.g., circular windings), the absolute value of the penetration depth can be calculated exactly by solving Maxwell's and London's equations with the usual magnetic field boundary conditions at an interface [16]. The large superconducting area and the flat coil geometry minimize cross-talk between the coils. The precision for detecting changes in λ is better than 0.5 Å. To adapt the experiment to the irradiation geometry with parallel tracks along specified directions, we used elongated *racetrack* coils instead of circular windings. These coils consist of straight sections of wire which were aligned parallel to the ion tracks as indicated in Fig. 1c. Since the screening current is a mirror image of the driving current, it is also driven parallel to the tracks within the undamaged superconductor and without intersecting and averaging material with different degrees of radiation damage. Because only parallel sections of the coils overlap, the irradiated window on both ends, the return currents perpendicular to the beam direction, are flowing through the non-irradiated film underneath the AuO_x layer. Since calculations depend on homogeneous film properties, the screening factor λ

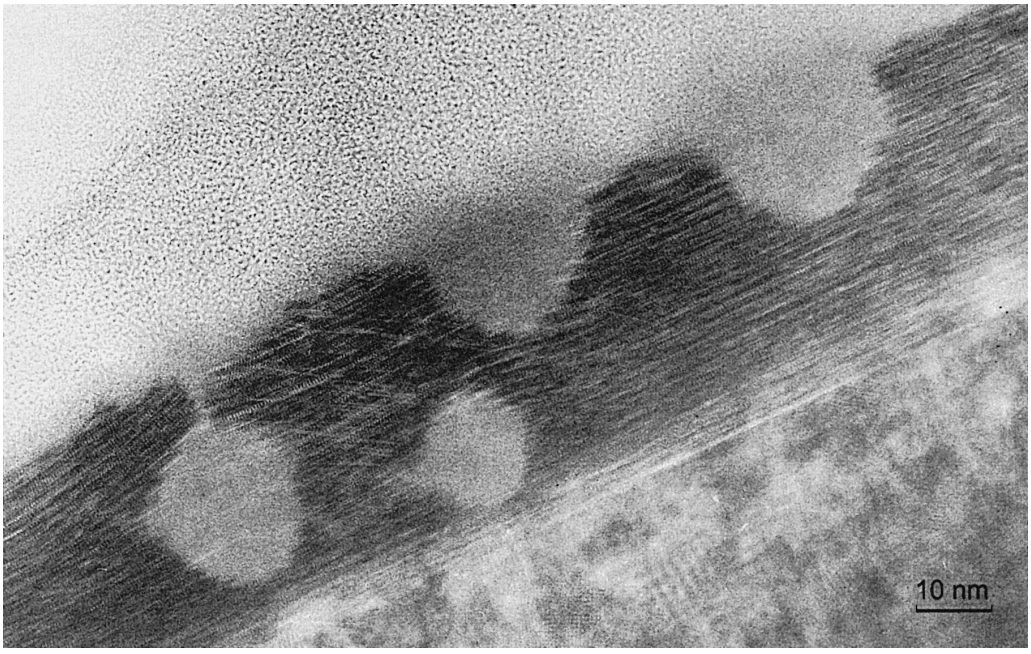

Fig. 2. The TEM cross-section of a 40-nm thick YBCO film irradiated with 10^{11} ions/cm^2 under grazing incidence. The transition between the amorphous core region (diameter 12–20 nm) and the surrounding undamaged crystalline material is abrupt within 1–2 nm. In this very thin film, the overlying YBCO material is partially cracked up above the tracks. This effect is strongly diminished in thicker films with cap layers as used for the measurement.

cannot be converted quantitatively into a penetration depth value. However, for small variations of λ, i.e., in the low temperature regime, the temperature dependences of $\lambda(T)$ and $S^{-1}(T)$ are the same except for a proportionality factor of order unity.

The overall behavior of the penetration depth below 25 K is depicted in Fig. 3. To compare different samples, the data have been normalized at 18 K. The choice of the normalization temperature does not play a role for the interpretation of the low temperature effects, as long as the normalization point is > 16 K. Each dataset represents three or four different samples irradiated in the same direction. In Fig. 3, we compare the temperature dependence of the penetration depth of films prior to irradiation with films irradiated at 0°, 22.5°, and 45° with respect to the axis of maximum order parameter (cf. Fig. 1b). The results can be summarized as follows: above 16 K, all the samples behave identically, demonstrating the excellent reproducibility of the experiment. However, in the low temperature regime below 15 K, the traces split and the penetration depth goes through a minimum between 6 and 8 K, increasing again with decreasing temperature.

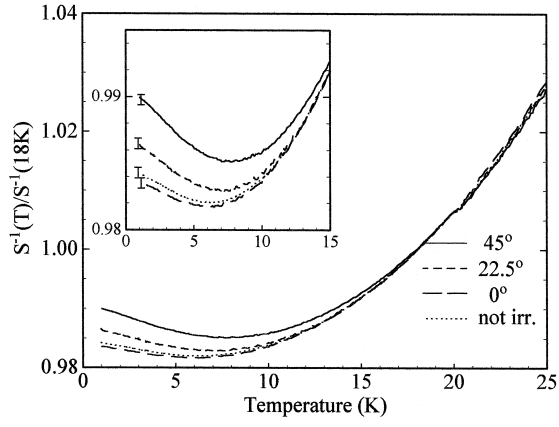

Fig. 3. Temperature dependence of penetration depth $\lambda \propto S^{-1}$ of YBCO films at low T. As grown films are compared to films containing ion tracks in three different directions. The strongest anomaly (upturn) is observed for tracks in [110] direction (45°). The inset shows an enlarged view of the low temperature region. The penetration depth is normalized for each sample by its value at 18 K.

Although the effect is very small ($\approx$ 0.3–0.5%), the precision is high enough to discriminate between the different irradiation directions. Within the experimental accuracy, films irradiated at 0° are indistinguishable from non-irradiated samples. With increasing angle, the minimum shifts slightly to higher temperatures (from 6 to 8 K) and the anomaly becomes stronger, reaching a maximum at 45°, i.e., current flow along the [110] direction. The most impressing and convincing evidence that the effect is directly correlated to the artificially generated internal surface layers is found by increasing their density. The result is depicted in Fig. 4a and b for tracks intersecting the film under 45° and 0° relative to the order parameter. For this experiment, the same films were repeatedly irradiated and inductively measured after each irradiation run. In this way, the track density was gradually increased from 0 up to $4.5 \times 10^{11}/\mathrm{cm}^2$. For the 45° direction, this led to a progressive enhancement of the low temperature anomaly nearly proportional to the total of the applied dose reaching upturn values of over 1% (Fig. 4a). In striking contrast, the same procedure had no significant effect at all in the 0° direction (Fig. 4b), where the low temperature behavior remained unchanged.

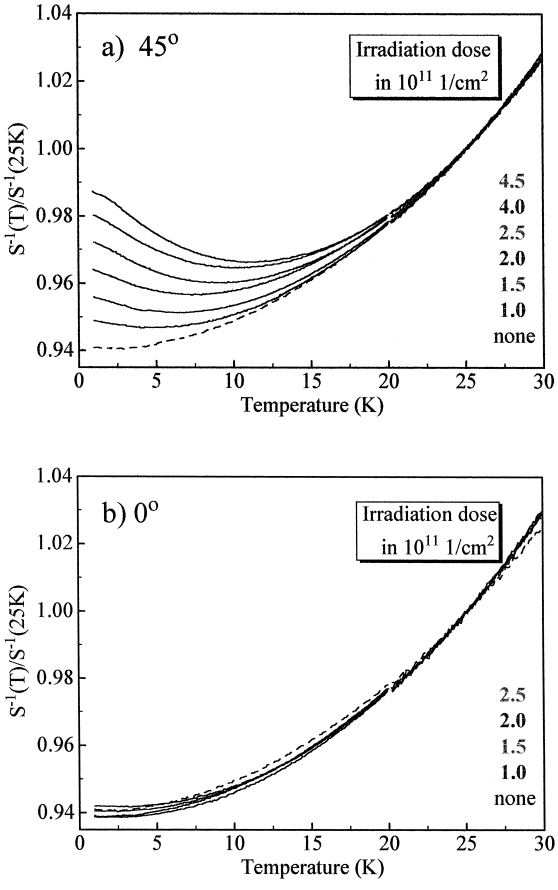

Fig. 4. Comparison of the low temperature behavior for tracks in [110] direction (45°) and [100] direction (0°) as a function of increasing track density, i.e., for increasing irradiation dose (from bottom to top). Data are normalized at 25 K.

An interpretation in terms of paramagnetic moments, e.g., located within the amorphous core of the tracks, is completely ruled out by the characteristic dependence of the anomalies on the irradiation direction. The existence of the anomaly and its strong correlation with the direction and density of the artificially produced boundaries can also not be explained by the standard theory of s-wave superconductivity. On the other hand, the d-wave model of superconductivity provides a natural interpretation of the AMCs in terms of current carrying ABSs at surfaces. These states are coherent mixtures of electrons and holes on the Fermi surface, and can be classified for clean superconductors and perfect surfaces by their momentum parallel to the surface. Two states with momenta $\pm \boldsymbol{p}_{\parallel}$ carry opposite currents and have the same energy in systems with time reversal symmetry. Hence, they are equally populated in thermal equilibrium and carry no net current. Time-reversal breaking perturbations such as a magnetic field split the energies of these states, resulting in an uneven population and a net equilibrium current. Of particular importance for the AMCs are zero-energy bound states associated with the sign changes of a d-wave order parameter on the Fermi surface [3–9,11,17]. The mechanism for forming the AMCs is the splitting, δ, of the zero-energy bound states caused either by a finite superflow with momentum, $\boldsymbol{p}_s = (\hbar/2\nabla\varphi - e/c\boldsymbol{A})$, or spontaneous time-reversal breaking by the surface order parameter, or both [5–7,11,17].

The surface currents can be calculated in the Fermi-liquid model of d-wave superconductivity [5–7,11,17]. This model covers, in general, correlation effects, bandstructure effects, and disorder such as surface roughness [8,9,18,19]. The calculated surface

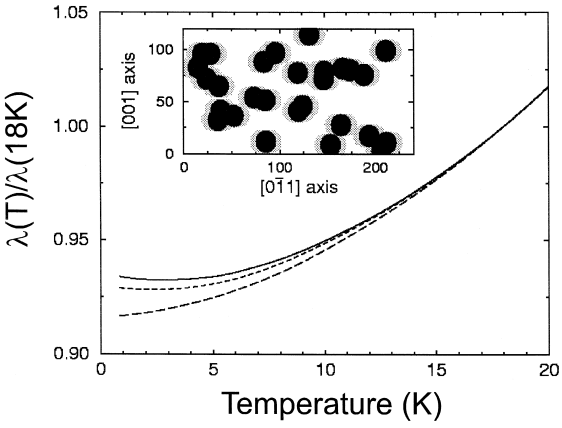

Fig. 5. Calculated temperature dependence of the effective penetration depth for channels at angle 45° (solid), 22.5° (short dashed), and 0° (long dashed). The results are obtained for a rough surface and a bulk inelastic broadening of the energies ($\hbar\tau_{in} = 0.02\,\Delta$). The inset shows a computer simulation of a random distribution of channels (black) of radius 10 nm and density 10^{11} cm^{-2}. The channels are surrounded by regions of anomalous screening currents (gray areas).

currents [20] were used as input to estimate the normalized screening factor for the experimental setup described above. We considered a representative random distribution of channels shown in Fig. 5, where channels describe the ion tracks and the disordered region around them. The channels are covered in the a–b planes by layers of width $\approx 4\xi_0$ (≈ 6 nm) of anomalous surface currents. The remaining bulk superconducting regions carry the regular Meissner current. From the screening factors, we obtain the effective penetration depth, $\lambda \propto S^{-1}$, for channels in [110] and [100] direction, i.e., 45° and 0°. Our results are shown in Fig. 5. The calculated difference between both directions is about 2% at 1 K for channels with rough surfaces and assuming an inelastic lifetime, $1/\tau_{in} = 0.02\,\Delta$. This result is in fairly good agreement with the experimental data shown in Fig. 3. We interpret the weaker T-dependence of the experimental data (in irradiated as well as non-irradiated samples) in comparison to the calculated ones as an effect of bulk pairbreaking by defects and natural grain boundaries. This effect is not included in our model calculations and reduces the linear T-dependence to a weak T^2-dependence. The large surface roughness needed to fit the data is reasonable in view of the transition region of ≈ 1–2 nm covering the amorphous channels.

Finally, we note that a close examination of Fig. 3 shows that even the non-irradiated, as grown, YBCO films exhibit a weak, but significant, anomaly in the penetration depth. This is true for all the films (more than 50) we have studied so far. Measurements on the same samples by an independent microwave resonator technique at 18 GHz yield identical results and confirm previous findings [21]. Films contain natural interfaces, e.g., grain boundaries, which can be expected to give rise to AMCs analogous to the anomalous currents reported here for irradiated samples. This may explain why the linear temperature dependence of the penetration depth predicted for ideal d-wave superconductors, and reported for pure YBCO single crystals [22], is usually not seen in YBCO films. We interpret the good qualitative agreement of our systematic measurements of the size and orientation dependence of the anomalous screening effect with the theory of ABSs in d-wave superconductors as an indication of the presence of current carrying ABSs at surfaces of YBCO.

Acknowledgements

The work of JAS was supported in part by the STC for Superconductivity through NSF Grant no. 91-20000. D.R. and J.A.S. also acknowledge support from the Max-Planck-Gesellschaft and the Alexander von Humboldt-Stiftung.

References

[1] V. Ambegaokar, P.G. de Gennes, D. Rainer, Phys. Rev. A 9 (1974) 2676.
[2] L.J. Buchholtz, G. Zwicknagl, Phys. Rev. B 23 (1981) 5788.
[3] C.-R. Hu, Phys. Rev. Lett. 72 (1994) 1526.
[4] Y. Tanaka, S. Kashiwaya, Phys. Rev. Lett. 74 (1995) 3451.
[5] M. Matsumoto, H. Shiba, J. Phys. Soc. Jpn. 64 (1995) 1703.
[6] M. Matsumoto, H. Shiba, J. Phys. Soc. Jpn. 64 (1995) 3384.
[7] M. Matsumoto, H. Shiba, J. Phys. Soc. Jpn. 64 (1995) 4867.
[8] L.J. Buchholtz et al., J. Low Temp. Phys. 101 (1995) 1079.
[9] L.J. Buchholtz et al., J. Low Temp. Phys. 101 (1995) 1099.
[10] M. Sigrist et al., Phys. Rev. Lett. 74 (1995) 3249.
[11] M. Fogelström et al., Phys. Rev. Lett. 79 (1997) 281.
[12] M. Covington et al., Phys. Rev. Lett. 79 (1997) 772.

[13] H. Hilgenkamp et al., Phys. Rev. B 53 (1996) 14586.
[14] F. Baudenbacher et al., Nucl. Instr. Mess. B 107 (1996) 327.
[15] P. Berberich et al., Physica C 219 (1994) 497.
[16] A. Fuchs et al., Phys. Rev. B 53 (1996) 14745.
[17] S. Higashitani, J. Phys. Soc. Jpn. 66 (1997) 2556.
[18] K. Yamada et al., J. Phys. Soc. Jpn. 96 (1996) 1540.
[19] Yu.S. Barash et al., Phys. Rev. B 55 (1997) 15282.
[20] N. Klein, C. Zuccaro, FZ Jülich, IFF, unpublished.
[21] H. Walter et al., Phys. Rev. Lett. 80 (1998) 3598.
[22] W.N. Hardy et al., Phys. Rev. Lett. 70 (1993) 3999.